Environmental Science & Technology

Article

Cite This: Environ. Sci. Technol. 2019, 53, 8447−8454

pubs.acs.org/est

Enhancing the Ion-Size-Based Selectivity of Capacitive Deionization Electrodes

Eric N. Guyes,[†] Tahel Malka,[‡] and Matthew E. Suss*[,†]

[†]Faculty of Mechanical Engineering and [‡]Faculty of Chemical Engineering, Technion − Israel Institute of Technology, Haifa 3200003, Israel

Supporting Information

ABSTRACT: Capacitive deionization (CDI) is an emerging water treatment technology often applied to brackish water desalination and water softening. Typical CDI cells consist of two microporous carbon electrodes sandwiching a dielectric separator, and desalt feedwater flowing through the cell by storing ions in electric double layers (EDLs) within charged micropores. CDI cells have demonstrated size-based ion selectivity wherein smaller hydrated ions are preferentially electrosorbed over larger hydrated ions. We demonstrate that such size-based selectivity can be substantially enhanced through the addition of chemical charge to micropores via surface functionalization. We develop a micropore EDL theory that includes both finite ion size effects and micropore chemical charge, which predicts such enhancements and elucidates that they result from denser counterion packing in micropores. With our experimental CDI cell, we desalted an electrolyte consisting of equimolar potassium (K^+) and lithium (Li^+) ions. We show that use of a surface-functionalized (oxidized) cathode significantly increased the electrosorption ratio of smaller K^+ to larger Li^+ compared to a cell with a pristine cathode, for example, from ∼1 to 1.84 for a charging voltage of 0.4 V. Our model predicts yet-higher electrosorption ratios are attainable, but our experimental cell suffered from significant cathode chemical charge degradation at applied voltages of ∼1 V.

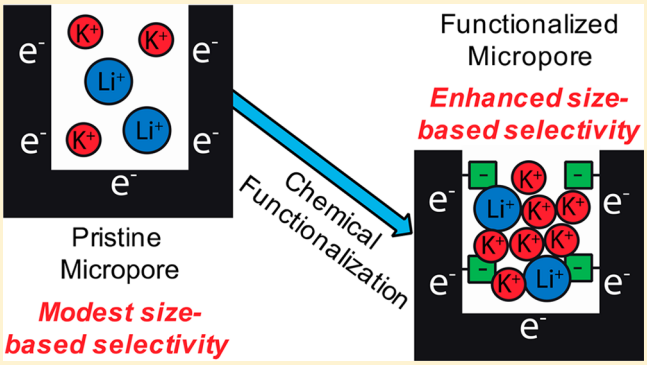

INTRODUCTION

Capacitive deionization (CDI) is an emerging water treatment technology investigated mainly toward brackish water desalination, but also for various alternate applications such as wastewater treatment, water softening, carbon dioxide capture, and organic solution deionization.[1−4] In CDI, desalination is performed by applying a voltage or current between a pair of electrodes, which are often microporous activated carbons, while feedwater flows through or between the electrodes.[1] Ions initially in the feedwater migrate to and are subsequently stored in electric double layers (EDLs) which form throughout the volume of charged micropores, a process known as electrosorption. Once the charging process is complete, the cell must be discharged and ions released into a brine stream, which is often accomplished by shorting the electrodes. In contrast to reverse osmosis (RO), CDI does not require high-pressure pumps or membranes, potentially enabling reduced infrastructure requirements and more readily downscalable systems for brackish water feeds. Typically, the feedwater flow is through a channel or spacer placed between the two static electrodes,[5−7] although a number of alternative cell architectures are currently under investigation, such as flow-through electrodes (Figure 1a),[5,8−10] membrane CDI,[11,12] and flowable electrode systems.[13−15] Other types of electrodes have emerged in recent years in addition to porous carbons, such as intercalation electrodes used in desalination batteries and hybrid CDI systems.[16−18]

In addition to quantifying performance metrics such as salt adsorption capacity (SAC) and cell energy efficiency,[1,19] experiments in CDI with microporous carbon electrodes have investigated selectively storing one or more ions over other competing (like-charged) ions. Valence-based selectivity has been shown, wherein CDI electrodes preferentially store ions with higher valence, such as Ca^{2+}, relative to competing ions with lower valence, like K^+.[20−22] Time-dependent selectivity has also been documented, occurring when one competing ion is initially preferred upon application of the cell voltage, but is gradually replaced by another ion when approaching cell equilibrium.[6,23] For example, when desalinating mixtures of Cl^- and NO_3^-, Chen et al. observed that Cl^- was stored at early charging times and desorbed slightly at later times, while NO_3^- was stored throughout charging.[23] Affinity-based selectivity, leveraging the affinity of electrode functional groups for particular ions, has been observed by several groups.[24−27] Dong et al. reported selective removal of Pb^{2+}

Received: December 10, 2018
Revised: June 6, 2019
Accepted: June 12, 2019
Published: June 12, 2019

DOI: 10.1021/acs.est.8b06954
Environ. Sci. Technol. 2019, 53, 8447−8454

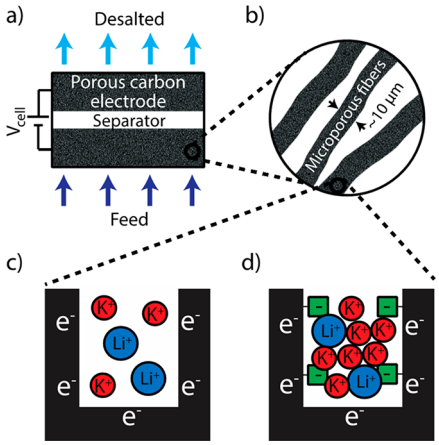

Figure 1. (a) Schematic of a flow-through electrode (FTE) CDI cell during cell charging, consisting of two electrically charged porous carbon electrodes and a dielectric separator. (b) Feedwater flows through the electrode, which consists of microporous woven carbon fibers. (c) A schematic of a micropore in a pristine cathode, with stored, competing, hydrated K^+ ions and larger hydrated Li^+ ions. (d) The cathode micropore functionalized with negatively charged surface groups. Relative to (c), in (d) the total counterion concentration is increased, resulting in enhanced size-based selectivity toward the K^+ ion.

over Ca^{2+} and Mg^{2+}, which they attributed to possible stronger bonding between the Pb^{2+} and the functional groups in the carbon electrode.[27] Furthermore, size-based selectivity has been reported between competing ions with the same valence, where generally the ion with the smaller hydrated size is preferentially stored.[21,28−33] While consistently observed, size-based selectivity generally results in modest electrosorption ratios, such as between 1.2 and 1.3 in favor of K^+ when competing with larger Na^+ ions at a cell voltage of 1−1.2 V.[21,31] Furthermore, CDI with microporous carbon electrodes has shown promise toward the selective removal of heavy metals[27,34] and excess nitrate.[23−25]

Despite the abundance of experimental studies that have reported selective ion removal in CDI, only a few theories have been proposed which capture data and explain selectivity mechanisms. Hou et al. presented Monte Carlo simulations capturing competitive ion electrosorption into charged nanopores, showing that ion valence governs selectivity at low surface charge densities while ion size plays an important role at high densities,[35] a result also obtained with mean-field theory by Biesheuvel et al. for planar EDLs.[36] For competing ions with different valences and bulk concentrations, Zhao et al. described the mechanisms underlying time-dependent selectivity, where at short charging times the electrosorption of each species is proportional to its relative concentration in the bulk, but at long charging times the species with higher valence is preferentially stored.[6] Suss developed theory describing a size-based selectivity mechanism, extending CDI theory with competing ions to account for ion volume exclusion interactions.[31] Oyarzun et al. modeled the inherent selectivity of NO_3^- relative to Cl^- in electrodes treated with cetyltrimethylammonium bromide (CTAB) by accounting for the equilibrium affinity between ionic species and surface groups.[25]

In parallel to studies on selectivity in CDI, surface functionalization of microporous carbons (adding chemical charge to micropores) has been explored toward improving SAC and cycle life. An early attempt by Cohen et al. reported a significant increase in charge efficiency by using a cathode oxidized in nitric acid because of a shifting of the electrode's point of zero charge (PZC) favorably for counterion electrosorption, although similar attempts to reduce the anode were not stable and an auxiliary electrode was required to control the anode potential.[37] Yang et al. later utilized carbon nanotubes functionalized with either negative sulfonic or positive amine groups to reduce co-ion expulsion, thereby increasing total salt removal, desalination rate, and charge efficiency.[38] Andelman reported similar findings with an anode functionalized with sodium dodecyl sulfate (SDS) and a cathode functionalized with hexadecyltrimethylammonium (HDTMA) bromide,[39] while Wu et al. reported enhanced performance with a cathode functionalized with nitric acid.[40] Subsequently, Gao et al. functionalized the anode with negatively charged groups and demonstrated inverted CDI, wherein desalination occurring during cell discharge resulted in improved CDI cell cycle life but also in reduced cell SAC.[41] In 2015, Biesheuvel et al. developed the theory of CDI including the effects of micropore chemical charge, which was able to predict features such as "inversion peaks" and "inverted CDI" and described a novel operational regime known as "extended voltage CDI",[42] which was subsequently confirmed experimentally by Gao et al.[43] In the latter work, the authors used a cathode functionalized with negatively charged carboxyl groups and an anode containing positive amine groups to achieved a nearly 2-fold increase in salt electrosorption and a significant boost in charge efficiency.[43] Hemmatifar et al. later extended CDI theory to include the pH dependence of chemical charge concentration on equilibrium salt storage.[44] Recently, Oyarzun et al. used a cell containing a quaternary amine-functionalized cathode and a benzenesulfonate-functionalized anode to preferentially remove NO_3^- over Cl^-, leveraging the inherent affinity of quarternary amine functional groups toward NO_3^-.[24,25]

In this work, we show that judicious use of chemical charge in CDI electrodes can lead to enhanced size-based selectivity. The mechanism we propose as underpinning this result is that chemical charging can increase the micropore counterion concentration for a given electric charge (illustrated schematically in Figure 1c,d), and counterion crowding results in stronger ion volume exclusion interactions and enhanced size-based selectivity. To demonstrate this concept, we develop the theory of ion electrosorption accounting for both ion size and electrode chemical charge, to the best of our knowledge for the first time in CDI. We present experimental results showing a significant increase in size-based selectivity when using a chemically charged (oxidized) cathode relative to the same cell with pristine (as-received) electrodes. Furthermore, we show that key trends seen in the measured electrosorption ratio are captured by theory, namely, the nonmonotonic dependence of electrosorption ratio on cell voltage. We report titration measurements indicating that the cathode chemical charge magnitude significantly decreased upon repeated cell cycling with charging voltages of around 1 V. Our theory predictions suggest yet-higher electrosorption ratios can be attained in the future if cathode chemical charge can be stabilized.

THEORY

We consider a two-electrode system in which each electrode is denoted by the subscript j, where j = A for the anode and j = C for the cathode. We consider an electrolyte with two cations

DOI: 10.1021/acs.est.8b06954
Environ. Sci. Technol. 2019, 53, 8447−8454

and one anion, where the cationic species are denoted by the subscript i = 1 or 2 and the anion by subscript i = co. To focus on size effects, we restrict the theory to monovalent ions with equal valence magnitude so that $z_1 = z_2 = -z_{co} = 1$. We further scale all potentials to the thermal voltage, $V_T = RT/F$, where R is the ideal gas constant, T is temperature, and F is the Faraday constant. To describe salt electrosorption in micropores with strongly overlapped EDLs, we employ the widely used Donnan approximation of spatially constant micropore potential.[6,30,31,42] Thus, for a given ion, equilibrium between the micropores and macropores yields

$$\ln(c_{\mathrm{mi},i,j}/c_{\mathrm{ma},i,j}) + \Delta\mu^{\mathrm{ex}}_{i,j} + z_i\Delta\phi_{\mathrm{D},j} = 0 \tag{1}$$

where $c_{\mathrm{mi},i,j}$ is the micropore concentration, $c_{\mathrm{ma},i,j}$ is the macropore concentration, $\Delta\mu^{\mathrm{ex}}_{i,j} = \mu^{\mathrm{ex,mi}}_{i,j} - \mu^{\mathrm{ex,ma}}_{i,j}$ is the excess potential difference between micropores and macropores, and $\Delta\phi_{\mathrm{D},j}$ is the nondimensional Donnan potential drop between the adjacent micropores and macropores.

The excess potential term in eq 1 can account for the departure of the solution from ideality due to finite ion size. We account here for ion size and ion volume exclusion interactions in the micropores and macropores by employing the Boublík−Mansoori−Carnahan−Starling−Leland (BMCSL) equation of state,[45,46] which treats ions as hard spheres. The BMCSL equation is for mixtures of spheres with differing diameters and reduces to the Carnahan−Starling equation for the case of uniform spheres and to the Bikerman equation for a point-size test particle in the presence of other ions with nonzero size.[36] It has been applied successfully to describe integrated properties of planar EDLs with ion mixtures,[36,47,48] and also has been applied to study size-based ion selectivity in confined micropore EDLs.[31]

In the micropores, the electric charge concentration is balanced by the ionic and chemical charge concentrations,

$$\sigma_{\mathrm{elec},j} + \sigma_{\mathrm{ionic},j} + \sigma_{\mathrm{chem},j} = 0 \tag{2}$$

where the ionic charge concentration is given by

$$\sigma_{\mathrm{ionic},j} = c_{\mathrm{mi},1,j} + c_{\mathrm{mi},2,j} - c_{\mathrm{mi,co},j} \tag{3}$$

In eq 2, $\sigma_{\mathrm{chem},j}$ accounts for the net charge concentration associated with charged groups in the micropores. As-received and surface-functionalized CDI electrodes generally possess both acidic and basic surface groups, and the net micropore chemical charge is obtained by summing together the contributions of positively and negatively charged groups.[44,49] Thus, $\sigma_{\mathrm{chem},j}$ is a function of the local micropore electrolyte pH as well as the local Donnan potential drop between micropores and macropores, and therefore $\sigma_{\mathrm{chem},j}$ can change dynamically during CDI cell charging.[44] However, we here restrict the model to a constant value of $\sigma_{\mathrm{chem},j}$, obtained for example at cell equilibrium, to simplify the model and focus on the effect of chemical charge on ion-size-based selectivity. The pH dependence of $\sigma_{\mathrm{chem},j}$ is included in a separate model used to interpret our titration data (see Supporting Information, Section 3). While ion size and chemical charge effects have been described in CDI in separate models,[31,42−44,50] to our knowledge this model is the first to include both effects concurrently, and their interplay toward enhanced size-based ion selectivity is elucidated.

The difference between the electrode potential ϕ_j and the macropore (bulk) potential $\phi_{\mathrm{ma},j}$ is related to Donnan and Stern potential drops via

$$\phi_j - \phi_{\mathrm{ma},j} = \Delta\phi_{\mathrm{D},j} + \Delta\phi_{\mathrm{S},j} \tag{4}$$

From the definition of the Stern layer capacitance C_S, the potential drop across the Stern layer is

$$\Delta\phi_{\mathrm{S},j} = -\frac{F}{V_T C_S}(\sigma_{\mathrm{ionic},j} + \sigma_{\mathrm{chem},j}) \tag{5}$$

where F is the Faraday constant. The total system charge is balanced according to

$$m_A\nu_{\mathrm{mi,A}}\sigma_{\mathrm{elec,A}} + m_c\nu_{\mathrm{mi,C}}\sigma_{\mathrm{elec,C}} = 0 \tag{6}$$

where $\nu_{\mathrm{mi,A}}$ and $\nu_{\mathrm{mi,C}}$ are the anode- and cathode-specific micropore volumes and m_A and m_C are the anode and cathode masses. For simplicity, for the rest of this work we will assume $m_A = m_C \equiv m/2$ and $\nu_{\mathrm{mi,A}} = \nu_{\mathrm{mi,C}} \equiv \nu_{\mathrm{mi}}$, so that eq 6 reduces to $\sigma_{\mathrm{elec,A}} + \sigma_{\mathrm{elec,C}} = 0$.[51] In a two-electrode system, the applied voltage ϕ is distributed between the two electrodes via

$$\phi - \phi_A + \phi_C = 0 \tag{7}$$

There are two typical modes for conducting CDI experiments, single-pass mode and batch mode.[52] For single-pass mode, eqs 1−7 can be solved simultaneously for equilibrium ion concentrations in the micropores of the anode and cathode at a given ϕ, assuming $c_{\mathrm{ma},i,j} = c_{\mathrm{feed},i}$, where $c_{\mathrm{feed},i}$ is the concentration of ion i in the feedwater. For single-pass charging, the electrosorption of ion i, Γ_i, is given by[51]

$$\Gamma_i = \frac{1}{2}\nu_{\mathrm{mi}}m(c^{\mathrm{f}}_{\mathrm{mi},i,C} - c^{0}{}_{\mathrm{mi},i,C} + c^{\mathrm{f}}_{\mathrm{mi},i,A} - c^{0}{}_{\mathrm{mi},i,A}) \tag{8}$$

Here, $c^0_{\mathrm{mi},i,j}$ is the micropore concentration of species i at the onset of charging and $c^{\mathrm{f}}_{\mathrm{mi},i,j}$ is the micropore concentration at the end of charging. While single pass is a common mode of operation, to study ion selectivity at equilibrium, it is often convenient to perform batch mode experiments. Here, a fixed volume of feedwater, V_{batch}, is recirculated through the cell during a charging or discharging half-cycle until equilibrium is reached. The batch's equilibrium ionic composition can then be analyzed off-line to study the achieved ion selectivity. For batch mode, the total number of moles of ion i is conserved between an initial state with $c_{\mathrm{batch},i} = c_{\mathrm{feed},i}$ and micropore concentrations $c^0_{\mathrm{mi},i,j}$, and a final state at the end of the half cycle with $c_{\mathrm{batch},i} = c_i$ and micropore concentrations $c^{\mathrm{f}}_{\mathrm{mi},i,j}$, via[51,53]

$$\frac{1}{2}\nu_{\mathrm{mi}}m(c^0_{\mathrm{mi},i,C} - c^{\mathrm{f}}_{\mathrm{mi},i,C} + c^0_{\mathrm{mi},i,A} - c^{\mathrm{f}}_{\mathrm{mi},i,A}) + V_{\mathrm{batch}}(c_{\mathrm{feed},i} - c_i) = 0 \tag{9}$$

We can also study a system charged in single-pass mode, and then discharged in batch mode. For this combined operation, eqs 1−7 must be solved simultaneously for $c^0_{\mathrm{mi},i,j}$, and then eqs 1−7 and eq 9 must be solved for $c^{\mathrm{f}}_{\mathrm{mi},i,j}$ and c_i. Then Γ_i can be calculated conveniently from the discharge half-cycle via

$$\Gamma_i = \frac{V_{\mathrm{batch}}}{m}|c_{\mathrm{feed},i} - c_i| \tag{10}$$

Figure 2 shows example predictions of the ion electrosorption ratio over single-pass charging, Γ_{K^+}/Γ_2, calculated using eq 8. The feedwater contains both K^+ (hydrated diameter 6.62 Å) and either Na^+ or Li^+ (hydrated diameter 7.16 or 7.64 Å, respectively).[54] Furthermore, ϕ = 40 (1.03 V at 25 °C) for charging and ϕ = 0 for discharging. For these calculations, we set $\sigma_{\mathrm{chem,A}} = 0$ and vary $\sigma_{\mathrm{chem,C}}$ to observe the predicted effect of negative chemical charge in the cathode

DOI: 10.1021/acs.est.8b06954
Environ. Sci. Technol. 2019, 53, 8447−8454

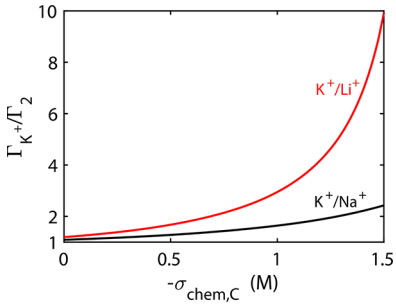

Figure 2. Predicted electrosorption ratio, Γ_{K^+}/Γ_2, versus cathode chemical charge concentration, $-\sigma_{chem,C}$, for a cell charged in single-pass mode. Calculations are for electrolytes with competing K^+/Na^+ (black curve) or K^+/Li^+ (red curve). Parameters include $\phi = 0$ initially and $\phi = 40$ (1.03 V at 25 °C) after cell charging, $C_S = 200$ F/mL, and $c_{feed,i} = c_{ma,i} = 2$ mM for each counterion.

micropores on selectivity. At $\sigma_{chem,C} = 0$, the predicted ion electrosorption ratios $\Gamma_{K^+}/\Gamma_{Na^+}$ and $\Gamma_{K^+}/\Gamma_{Li^+}$ are 1.09 and 1.19, respectively, indicating a modest preference toward the smaller K^+ ion. As can be seen in Figure 2, the model predicts that K^+ is more strongly preferred as we increase the magnitude of the cathode chemical charge, reaching a factor of 2.43 for K^+/Na^+ and 9.91 for K^+/Li^+ for $\sigma_{chem,C} = -1.5$ M. This strong enhancement in size-based separation is due largely to increased counterion concentrations and ion volume exclusion interactions in the cathode micropores upon adding chemical charge (see Figure 1 and Figure S1, Supporting Information). The difference in predicted electrosorption ratios of K^+/Na^+ and K^+/Li^+ for a given chemical charge concentration is due to the larger size disparity between K^+ and Li^+ relative to that between K^+ and Na^+.

MATERIALS AND METHODS

The electrodes used in this work were activated carbon cloth (ACC-5092-15, Kynol Europa GmbH, Germany) (Figure S2a) and were ~500 μm thickness each, with ~1500 m^2/g surface area as measured via N_2 adsorption (see Supporting Information, Section 2). This material was characterized in several previous CDI works.[19,37,55] The specific micropore volume was approximately 0.58 mL/g as determined from the N_2 adsorption data (see Figure S2b). Electrode material used without surface functionalization (as-received) is referred to as "pristine", while material that was subjected to an oxidation treatment is referred to as "oxidized". All electrodes were first cut to a size of 1.75 cm × 1.75 cm. The pristine electrodes were then rinsed with deionized (DI) water (18.2 MΩ, Synergy Water Purification System, Merck Millipore KGaA), dried in air at 80 °C overnight, and then weighed. The electrodes to be oxidized were immersed in 70% nitric acid for 24 h to affix negatively charged carboxyl groups into the micropores,[43] followed by a washing in 0.1 M sodium bicarbonate until the surface pH reached approximately 9, as measured with pH strips (Merck). The electrodes were then washed in DI water until the surface pH reached ~7, dried in air at 80 °C overnight, and then weighed. Electrodes were imaged using a high-resolution scanning electron microscope (SEM, Ultra Plus, Carl Zeiss NTS GmbH, Germany) and atomic composition was determined by energy-dispersive X-ray spectroscopy (EDS) in the same system (Tables S1 and S2).

We used direct titrations of our carbon electrodes to quantify their micropore chemical charge concentration.[43,44] The electrodes were ground in a mortar and pestle and then added to a vessel containing 19.35 mL of 0.05 M NaOH. Deionized (DI) water (62 mL) was added to raise the liquid level to cover the pH electrode. A small volume of 0.05 M HCl (7.6 mL for pristine electrodes, 0.5 mL for oxidized electrodes) was added to the vessel to bring the initial solution pH closer to 10, the upper limit of the range of interest. A smaller HCl volume was added to the oxidized electrodes because the negative surface groups deprotonate in the presence of the NaOH, thus reducing the initial pH. The solution was sparged with nitrogen until the measured dissolved oxygen content decreased to ~5% of saturation (Orion Star A213, Thermo Fisher Scientific, USA), then sealed, and left undisturbed for 5 days under stirring. The solution was then transferred to a 150 mL vessel in a titration system (Titrando 904 and iAquatrode Plus Pt1000, Metrohm AG, Switzerland) and sparged with nitrogen for an additional 20 min. The nitrogen flow was then reduced to one bubble every several seconds to maintain positive pressure in the vessel and prevent air intrusion. The resulting solution was automatically titrated with 60 mL of 0.05 M HCl with a potential drift criterion of 0.05 mV/min. A control titration without the electrode material was executed with the same protocol (and an initial HCl volume of 7.6 mL as with the pristine electrode). Measured equilibrium pH versus added titrant volume curves are given in Figure S3 in the Supporting Information, and we determined the total chemical charge concentration in the micropores via fitting the experimental data to a suitable model (see Supporting Information, Section 3).[44]

A description and schematic of our custom-built flow-through electrodes (FTE) CDI cell are given in a previous publication,[9] and further details are given in Supporting Information, Section 4. Feedwater comprised of 2 mM KCl (KCl salt, >99.5% purity, Merck Millipore KGaA, Germany) and 2 mM LiCl (LiCl salt, >99% purity, Acros Organics, Belgium) was prepared with DI water. The solution was sparged with nitrogen gas in a 0.5 L glass reservoir until the dissolved oxygen level decreased to ~5% of saturation. A peristaltic pump (Masterflex 07551-30, Cole Parmer, USA) supplied the feedwater at a rate of 1 mL/min to the CDI cell. To condition the cell and reach the limit cycle, we performed five 1-h-long cycles in single-pass configuration, with a charging voltage matching that of the subsequent experiment and discharging at 0 V. Effluent conductivity was measured via a flow-through conductivity sensor (Tracedec 390-50, Innovative Sensor Technologies GmbH, Austria).

After conditioning, single-pass cell charging was carried out at a constant voltage of either 0.4, 0.6, 0.8, 1.0, or 1.2 V until equilibrium was reached (~2−2.5 h). After reaching equilibrium and with the charging voltage still applied, the system was switched to a batch configuration containing 9 mL of feedwater. The cell was then discharged at 0 V until the batch solution conductivity reached a steady value and the current magnitude was less than 0.1 mA, whereupon the batch solution was extracted for measurement of the electrosorption ratio (see Figure S4). Note that, typically, ion electrosorption is calculated after the CDI cell charges to equilibrium.[5,32] However, it is well-characterized that during cell charging the macropore and effluent solution pH can deviate strongly from that of the feedwater, even at equilibrium, and especially at high cell voltages of ~1 V.[56] Thus, during charging the

DOI: 10.1021/acs.est.8b06954
Environ. Sci. Technol. 2019, 53, 8447−8454

potentially significant contribution of H^+ to the effluent ionic conductivity and the effect of pH gradients on the effective electrode surface charge can complicate the analysis. In contrast, for discharging at a cell voltage of 0 V, the effluent pH at equilibrium is typically about equal to the feedwater pH,[57] which is why we here calculate ion electrosorption from cell discharge. Experiments were performed for either pristine−pristine or oxidized−pristine cathode−anode pairs, and electrodes were replaced with a fresh pair after completing experiments for one charging voltage. The pH of the batch solutions was checked post-experiment by extracting a droplet from each solution with a pipet and dropping it onto a pH strip. The batch pH was found to be near-neutral in each case, showing that the influence of H^+ and OH^- on the ionic conductivity was negligible.

The batch solutions collected after cell discharge were diluted with deionized water to obtain a sufficiently large volume (50 mL) for selectivity measurements, and an ionic strength adjuster (ISA) consisting of concentrated NaCl (Thermo Fisher) was added in a ratio of 1 mL of ISA to 50 mL of sample to fix the activity coefficient between different solutions. A reference solution containing fresh feedwater was prepared similarly. A K^+ ion selective electrode (6.0510.110, Metrohm) was calibrated as described in the Supporting Information, Section 5. The K^+ concentrations of the reference and sample solutions were then measured with the ion selective electrode and corrected for temperature variations, and the electrode was rinsed in DI for 20−30 s between each measurement. After the K^+ concentration was measured, the Li^+ concentration was calculated from the measured ionic conductivity, κ, of the batch solution after cell discharge. For this, we used equivalent molar conductivities Λ_{KCl} = 0.143 mS/cm/mM and Λ_{LiCl} = 0.109 mS/cm/mM[58] and calculated the Li^+ concentrations via

$$c_{Li^+} = (\kappa - c_{K^+}\Lambda_{KCl})/\Lambda_{LiCl} \quad (11)$$

RESULTS AND DISCUSSION

Figure 3a shows the micropore chemical charge concentration for an unused pristine electrode and an unused oxidized electrode versus solution pH, obtained from fitting a model to titration data (Supporting Information, Section 3). As can be seen, at pH 3, the chemical charge concentrations of the pristine and oxidized electrodes are calculated to be +0.27 and +0.07 M, respectively. As pH increases, the pristine electrode chemical charge decreases slowly, reaching −0.46 M at pH 10. In contrast, the oxidized electrode chemical charge decreases much more sharply with increasing pH, reaching −1 M at pH 6.55 and −2.73 M at pH 10. The latter indicates that oxidation raised significantly the micropore concentration of surface groups that behave as weak acids, such as carboxyl groups.[10,43] We also note that, for pH > 6, the chemical charge concentration profiles in Figure 3a are qualitatively similar to results obtained by Gao et al. for activated carbon cloth oxidized in nitric acid.[43] In Figure 3b−d, we show results from single-pass charging/batch-mode discharging characterization experiments of our CDI cell, when using a 2 mM LiCl and 2 mM KCl mixture as the feedwater. In Figure 3b we plot electric charge stored at the limit cycle, q, for charging voltages, V_{cell}, ranging from 0.4 to 1.2 V, and with a discharge voltage of 0 V. We show results for a cell with two pristine electrodes (black diamonds) and with a pristine anode and an oxidized cathode (red circles). We calculate q from our CDI

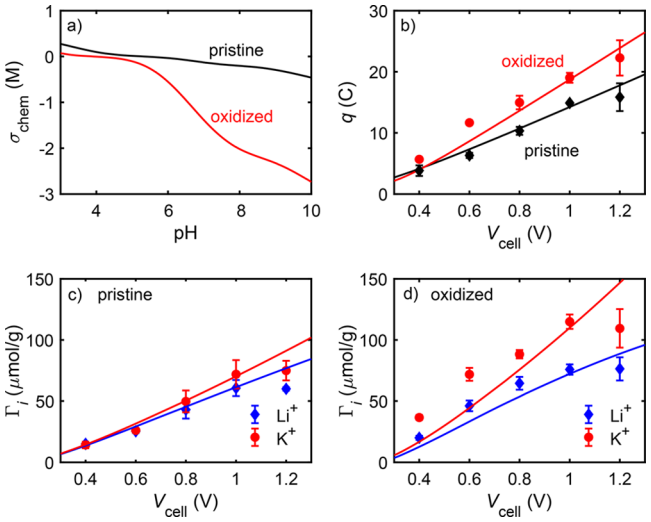

Figure 3. (a) Micropore chemical charge concentration, σ_{chem}, for pristine and oxidized electrodes versus feed pH, obtained from titration model-to-data fitting. (b) Theory (lines) and measurements (markers) of charge stored, q, versus V_{cell} for a cell with either a pristine cathode or an oxidized cathode. (c) Theory (lines) and measurements (markers) of electrosorption, Γ_i, of the pristine cathode cell toward K^+ (red circles) and Li^+ (blue diamonds) versus V_{cell}. (d) Theory (lines) and measurements (markers) of Γ_i for Li^+ and K^+ versus V_{cell} for the cell with an oxidized cathode. Theory lines are for $\sigma_{chem,C}$ = −0.75 M and $\sigma_{chem,A}$ = −0.05 M. Error bars represent 95% confidence intervals determined from at least three realizations.

experiments by integrating the measured current in time over the discharge half-cycle. As can be seen, the capacitance of the cell with an oxidized cathode is larger at all cell voltages tested here. Gao et al. similarly reported increased cell capacitance when using an oxidized cathode relative to an untreated cathode,[43] though Wu et al. showed a slightly lower capacitance for their cell with an oxidized cathode.[40]

Solid lines in Figure 3b represent model predictions (see Theory section) for the case of pristine electrodes (black line) and a cell with a pristine anode and an oxidized cathode (red line). These are calculated via $q = (1/2)F\nu_{mi}|\sigma_{elec,j} - \sigma^0_{elec,j}|$,[51] where ν_{mi} = 0.58 mL/g (see Supporting Information, Section SI-2), and $\sigma^0_{elec,j}$ is the micropore electric charge concentration present in the electrode at 0 V, which is not necessarily zero because of the presence of chemical charge in the cathode. The total cell electrode mass m used in the model was 0.5 g for all curves. The Stern layer capacitance, C_S, was used as a fitting parameter to fit the model to the data in Figure 3b. The fitted Stern capacitances for the pristine and oxidized cathode cells are 135 and 200 F/mL, respectively, comparable to our previous work with pristine Kynol electrodes in 5 and 20 mM NaCl that yielded a value of 145 F/mL.[9] The experimental data generally follow the trends predicted by the fitted model, though deviating somewhat for V_{cell} = 1.2 V.

Figure 3c displays measured values of Γ_i for K^+ (red circles) and Li^+ (blue diamonds) for the cell with pristine electrodes at charging voltages of 0.4−1.2 V. After cell discharge, we measured c_{K^+} from the batch volume using an ion-selective electrode, while c_{Li^+} was determined with eq 11 and then Γ_i values were calculated via eq 10. In Figure 3c we observe that the measured Γ_{K^+} is about equal to or slightly higher than Γ_{Li^+} at all cell voltages tested. The latter observations are consistent with a size-based selectivity mechanism, as K^+ has a smaller

DOI: 10.1021/acs.est.8b06954
Environ. Sci. Technol. 2019, 53, 8447−8454

hydrated radius than Li^+.[31] Solid lines in Figure 3c represent model predictions and were obtained using $\sigma_{chem,A} = \sigma_{chem,C} = -0.05$ M as fitting parameters to the data. The value used is consistent with the independent measurements of chemical charge concentration shown in Figure 3a for a feedwater pH of 6.2.

The measured ion electrosorption for the cell with an oxidized cathode is shown in Figure 3d, for K^+ (red circles) and Li^+ (blue diamonds) and for charging voltages of 0.4−1.2 V. The electrosorption of each species is higher than that of the pristine cathode cell shown in Figure 3c for the same cell voltage, which is consistent with previous studies comparing the performance of cells with either oxidized or pristine cathodes.[40,43] This increase in electrosorption is attributed to the shifting of the electric charge compensation mechanism more strongly toward counterion electrosorption in the oxidized cathode.[37,42] Additionally, we observe a much larger separation between measured Γ_{K^+} and Γ_{Li^+} at all cell voltages relative to the results shown in Figure 3c, indicating a greater electrosorption ratio when using the oxidized cathode. Lines represent an example model result with $\sigma_{chem,A} = -0.05$ M as used in Figure 3c, and for $\sigma_{chem,C} = -0.75$ M. We observe that K^+ electrosorption by the experimental cell is significantly larger than the model predictions at 0.4 and 0.6 V, but about equal to model predictions at 1 V.

In Figure 4, we show the electrosorption ratio, $\Gamma_{K^+}/\Gamma_{Li^+}$, where black diamonds denote the measured ratio for the cell with a pristine cathode and red circles for the cell with an oxidized cathode. For the cell with the pristine cathode, $\Gamma_{K^+}/\Gamma_{Li^+}$ is 0.94 at $V_{cell} = 0.4$ V and rises with increasing voltage, reaching 1.19 at 1 V and 1.25 at 1.2 V. This is consistent with the trends previously reported in similar systems with unmodified carbon electrodes. For example, when desalting a feed solution of 5 mM NaCl and 5 mM KCl, Dykstra et al. observed a factor of ∼1.3 for K^+ relative to Na^+ for a charge voltage of 1 V.[29] For a feed solution of 2 mM NaCl and 2 mM KCl and charging at 1.2 V, Hou and Huang reported a factor of ∼1.22 in favor of K^+ relative to Na^+.[21] As can be seen in Figure 4, the measured $\Gamma_{K^+}/\Gamma_{Li^+}$ for the cell with an oxidized cathode is larger than that for the pristine cathode case at all cell voltages tested, demonstrating an enhanced size-based ion separation. Furthermore, the trend in $\Gamma_{K^+}/\Gamma_{Li^+}$ with cell voltage is distinctly nonmonotonic, with the highest measured value of 1.84 at $V_{cell} = 0.4$ V, followed by a decrease to a minimum of 1.37 at 0.8 V, and then followed by a slight increase to 1.52 at 1 V. To our knowledge, these latter measurements are the first reports of electrosorption ratio for equal-valence, competing cations in a CDI cell with an oxidized cathode.

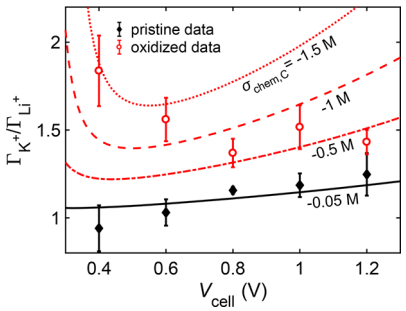

Figure 4. Experimentally measured and theoretically predicted electrosorption ratios, $\Gamma_{K^+}/\Gamma_{Li^+}$, for a CDI cell with a pristine cathode (black diamond markers, black line) or an oxidized cathode (red circle markers, broken red lines). Error bars represent 95% confidence intervals calculated from at least three realizations.

Model calculations of $\Gamma_{K^+}/\Gamma_{Li^+}$ for a cell with pristine electrodes (black line, $\sigma_{chem,A} = \sigma_{chem,C} = -0.05$ M) follow the trend in the experimental data of increasing electrosorption ratio with voltage. For the cell with an oxidized cathode, we plot several theory curves with varying values of $\sigma_{chem,C}$ and a fixed value of $\sigma_{chem,A} = -0.05$ M (red lines), and all theory curves show a distinctly nonmonotonic trend also seen in the data. The predicted $\Gamma_{K^+}/\Gamma_{Li^+}$ curves all decrease with increasing V_{cell} to a minimum around 0.4−0.5 V, after which they increase with increasing V_{cell}. The theoretical prediction and experimental observation of the largest $\Gamma_{K^+}/\Gamma_{Li^+}$ at low V_{cell} is a counterintuitive result, given that ion volume exclusion interactions in the cathode increase monotonically with electrode voltage. However, this observation is likely due to the relative importance of cation expulsion from the anode at low cell voltages, which results in very low Γ_{Li^+} and so high $\Gamma_{K^+}/\Gamma_{Li^+}$ (see Supporting Information, Section 6). We further observe that the data at the lowest V_{cell} best fit the theory curve with highest chemical charge concentration, $\sigma_{chem,C} = -1.5$ M, but at higher V_{cell} the fit is better for $\sigma_{chem,C} = -0.5$ M. From titration results plotted in Figure 3a, we obtain $\sigma_{chem,C} = -1.4$ M at pH 7, a value roughly equal to that which provides best fit to data in Figure 4 at 0.4 V.

We return to the discrepancy between model and data for the cell with an oxidized cathode in Figures 3d and 4. In these plots, a single value of $\sigma_{chem,C}$ does not adequately capture all of the experimental points, and generally lower values of $\sigma_{chem,C}$ than those measured independently (Figure 3a) are needed to capture data at high V_{cell} of 0.8−1.2 V. One possible explanation is the presence of acidified electrolyte in the cathode micropores at higher voltages, which would render much of the carboxylic acid groups in the cathode micropores neutrally charged. However, this cause is unlikely as pH in the cathode macropores at the end of batch-mode discharging is about equal to the feedwater pH (see Materials and Methods). Another explanation is the possible degradation of the net chemical charge in the cathode during the CDI experiments, as no stability tests of CDI cells with oxidized cathodes have been reported to our knowledge. We tested this explanation by performing ex situ direct titrations of the cathode electrode after it had been used in the CDI experiments shown in Figures 3b−d and 4. The net micropore chemical charge concentration versus pH, obtained from titration model-to-data fitting, is shown in Figure 5 (see Supporting Information, Section 3, for fitting details). As can be seen, relative to the $\sigma_{chem,C}$ obtained for the oxidized electrode pre-experiment (shown also in Figure 3a), all post-experiment electrodes show significant reductions in negative chemical charge concentration at all pH values tested. The magnitude of the reduction is a strong function of the cell voltage applied in the preceding CDI experiments, with a relatively slight reduction for 0.4 V, and a much more dramatic reduction for 1.2 V. For example, at pH 7, the measured chemical charge is reduced from −1.4 M initially to −1.1 M after the 0.4 V experiments, and to −0.3 M after the 1.2 V experiments. Gao et al. similarly noticed that cells with oxidized cathodes do not perform as well as expected given the measured negative chemical charge concentration,[43] but did not propose or identify cathode surface charge degradation during CDI cell cycling as a potential cause. Thus, to our knowledge, our results are the first demonstration of the

DOI: 10.1021/acs.est.8b06954
Environ. Sci. Technol. 2019, 53, 8447−8454

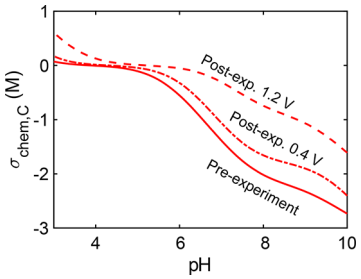

Figure 5. Micropore chemical charge concentration, $\sigma_{chem,C}$, versus solution pH, of oxidized cathodes for both pre- and post-CDI experiments, obtained from titration model-to-data fitting. Results are shown for the oxidized material before use in CDI experiments (solid line), and post-experiment where the cell charging voltage was either 0.4 (dashed-dotted line) or 1.2 V (dashed line).

reduction of an oxidized cathode's negative chemical charge concentration upon CDI cell cycling. The mechanism underpinning this reduction has not yet been elucidated, but should be the subject of a future work. We suspect that significantly higher values of $\Gamma_{K^+}/\Gamma_{Li^+}$ can be attained experimentally if the cathode chemical charge is not degraded at high cell voltage.

■ ASSOCIATED CONTENT

Supporting Information

The Supporting Information is available free of charge on the ACS Publications website at DOI: 10.1021/acs.est.8b06954.

Predictions of micropore selectivity for pristine and oxidized cathodes; electrode material characterization; titration protocol and chemical charge determination; CDI cell and experiment details; conductivity and K^+ electrode calibration details; additional details for nonmonotonic electrosorption ratio are shown in Figure S6 (PDF)

■ AUTHOR INFORMATION

Corresponding Author

*E-mail: mesuss@me.technion.ac.il.

ORCID

Eric N. Guyes: 0000-0002-2720-464X

Notes

The authors declare no competing financial interest.

■ ACKNOWLEDGMENTS

The authors would like to acknowledge the support of the Planning & Budgeting Committee/Israel Council for Higher Education (CHE) and Fuel Choice Initiative (Prime Minister Office of Israel), within the framework of "Israel National Research Center for Electrochemical Propulsion" (INREP). SEM photography and EDS were performed by Dr. Alexander Berner and Dr. Anna Kosinova. Nitrogen adsorption measurements and analysis were carried out by Dr. Dina Spasser in the laboratory of Prof. Oz Gazit. Blank titration carried out by Yinke Chen. We are grateful to Dr. Slawomir Porada and Dr. Anica Lancuški for helpful discussions regarding titrations with carbon electrodes.

■ REFERENCES

(1) Suss, M. E.; Porada, S.; Sun, X.; Biesheuvel, P. M.; Yoon, J.; Presser, V. Water Desalination via Capacitive Deionization: What Is It and What Can We Expect from It? *Energy Environ. Sci.* **2015**, *8* (8), 2296−2319.

(2) Seo, S. J.; Jeon, H.; Lee, J. K.; Kim, G. Y.; Park, D.; Nojima, H.; Lee, J.; Moon, S. H. Investigation on Removal of Hardness Ions by Capacitive Deionization (CDI) for Water Softening Applications. *Water Res.* **2010**, *44* (7), 2267−2275.

(3) Legrand, L.; Schaetzle, O.; de Kler, R. C. F.; Hamelers, H. V. M. Solvent-Free CO2 Capture Using Membrane Capacitive Deionization. *Environ. Sci. Technol.* **2018**, *52* (16), 9478−9485.

(4) Porada, S.; Feng, G.; Suss, M. E.; Presser, V. Capacitive Deionization in Organic Solutions: Case Study Using Propylene Carbonate. *RSC Adv.* **2016**, *6* (7), 5865−5870.

(5) Remillard, E. M.; Shocron, A. N.; Rahill, J.; Suss, M. E.; Vecitis, C. D. A Direct Comparison of Flow-by and Flow-through Capacitive Deionization. *Desalination* **2018**, *444*, 169−177.

(6) Zhao, R.; van Soestbergen, M.; Rijnaarts, H. H. M.; van der Wal, A.; Bazant, M. Z.; Biesheuvel, P. M. Time-Dependent Ion Selectivity in Capacitive Charging of Porous Electrodes. *J. Colloid Interface Sci.* **2012**, *384* (1), 38−44.

(7) Hemmatifar, A.; Stadermann, M.; Santiago, J. G. Two-Dimensional Porous Electrode Model for Capacitive Deionization. *J. Phys. Chem. C* **2015**, *119* (44), 24681−24694.

(8) Qu, Y.; Campbell, P. G.; Hemmatifar, A.; Knipe, J. M.; Loeb, C. K.; Reidy, J. J.; Hubert, M. A.; Stadermann, M.; Santiago, J. G. Charging and Transport Dynamics of a Flow-Through Electrode Capacitive Deionization System. *J. Phys. Chem. B* **2018**, *122* (1), 240−249.

(9) Guyes, E. N.; Shocron, A. N.; Simanovski, A.; Biesheuvel, P. M.; Suss, M. E. A One-Dimensional Model for Water Desalination by Flow-through Electrode Capacitive Deionization. *Desalination* **2017**, *415*, 8−13.

(10) Avraham, E.; Noked, M.; Bouhadana, Y.; Soffer, A.; Aurbach, D. Limitations of Charge Efficiency in Capacitive Deionization Processes III: The Behavior of Surface Oxidized Activated Carbon Electrodes. *Electrochim. Acta* **2010**, *56* (1), 441−447.

(11) Biesheuvel, P. M.; Zhao, R.; Porada, S.; van der Wal, A. Theory of Membrane Capacitive Deionization Including the Effect of the Electrode Pore Space. *J. Colloid Interface Sci.* **2011**, *360* (1), 239−248.

(12) Tang, W.; He, D.; Zhang, C.; Waite, T. D. Optimization of Sulfate Removal from Brackish Water by Membrane Capacitive Deionization (MCDI). *Water Res.* **2017**, *121* (Mcdi), 302−310.

(13) Jeon, S., II; Park, H. R.; Yeo, J. G.; Yang, S.; Cho, C. H.; Han, M. H.; Kim, D. K. Desalination via a New Membrane Capacitive Deionization Process Utilizing Flow-Electrodes. *Energy Environ. Sci.* **2013**, *6* (5), 1471−1475.

(14) Doornbusch, G. J.; Dykstra, J. E.; Biesheuvel, P. M.; Suss, M. E. Fluidized Bed Electrodes with High Carbon Loading for Water Desalination by Capacitive Deionization. *J. Mater. Chem. A* **2016**, *4* (10), 3642−3647.

(15) Rommerskirchen, A.; Gendel, Y.; Wessling, M. Single Module Flow-Electrode Capacitive Deionization for Continuous Water Desalination. *Electrochem. Commun.* **2015**, *60*, 34−37.

(16) Yang, J.; Zou, L.; Song, H.; Hao, Z. Development of Novel MnO2/Nanoporous Carbon Composite Electrodes in Capacitive Deionization Technology. *Desalination* **2011**, *276* (1−3), 199−206.

(17) Smith, K. C.; Dmello, R. Na-Ion Desalination (NID) Enabled by Na-Blocking Membranes and Symmetric Na-Intercalation: Porous-Electrode Modeling. *J. Electrochem. Soc.* **2016**, *163* (3), A530−A539.

(18) Srimuk, P.; Lee, J.; Fleischmann, S.; Aslan, M.; Kim, C.; Presser, V. Potential-Dependent, Switchable Ion Selectivity in Aqueous Media Using Titanium Disulfide. *ChemSusChem* **2018**, *11* (13), 2091−2100.

(19) Kim, C.; Srimuk, P.; Lee, J.; Fleischmann, S.; Aslan, M.; Presser, V. Influence of Pore Structure and Cell Voltage of Activated Carbon Cloth as a Versatile Electrode Material for Capacitive Deionization. *Carbon* **2017**, *122*, 329−335.

(20) Li, Y.; Zhang, C.; Jiang, Y.; Wang, T. J.; Wang, H. Effects of the Hydration Ratio on the Electrosorption Selectivity of Ions during Capacitive Deionization. *Desalination* **2016**, *399*, 171−177.

DOI: 10.1021/acs.est.8b06954
Environ. Sci. Technol. 2019, 53, 8447−8454

(21) Hou, C.; Huang, C. Y. A Comparative Study of Electrosorption Selectivity of Ions by Activated Carbon Electrodes in Capacitive Deionization. *Desalination* **2013**, *314*, 124−129.
(22) Huang, S. Y.; Fan, C. S.; Hou, C. H. Electro-Enhanced Removal of Copper Ions from Aqueous Solutions by Capacitive Deionization. *J. Hazard. Mater.* **2014**, *278*, 8−15.
(23) Chen, Z.; Zhang, H.; Wu, C.; Wang, Y.; Li, W. A Study of Electrosorption Selectivity of Anions by Activated Carbon Electrodes in Capacitive Deionization. *Desalination* **2015**, *369*, 46−50.
(24) Oyarzun, D. I.; Hemmatifar, A.; Palko, J. W.; Stadermann, M.; Santiago, J. G. Adsorption and Capacitive Regeneration of Nitrate Using Inverted Capacitive Deionization with Surfactant Functionalized Carbon Electrodes. *Sep. Purif. Technol.* **2018**, *194*, 410−415.
(25) Oyarzun, D.; Palko, J.; Stadermann, M.; Santiago, J.; Hemmatifar, A. Ion Selectivity in Capacitive Deionization with Functionalized Electrode: Theory and Experimental Validation. *Water Research X* **2018**, *1*, 100008.
(26) Su, X.; Tan, K. J.; Elbert, J.; Rüttiger, C.; Gallei, M.; Jamison, T. F.; Hatton, T. A. Asymmetric Faradaic Systems for Selective Electrochemical Separations. *Energy Environ. Sci.* **2017**, *10* (5), 1272−1283.
(27) Dong, Q.; Guo, X.; Huang, X.; Liu, L.; Tallon, R.; Taylor, B.; Chen, J. Selective Removal of Lead Ions through Capacitive Deionization: Role of Ion-Exchange Membrane. *Chem. Eng. J.* **2019**, *361* (July), 1535−1542.
(28) Gabelich, C. J.; Tran, T. D.; Suffet, I. H. M. Electrosorption of Inorganic Salts from Aqueous Solution Using Carbon Aerogels. *Environ. Sci. Technol.* **2002**, *36* (13), 3010−3019.
(29) Dykstra, J. E.; Dijkstra, J.; van der Wal, A.; Hamelers, H. V. M.; Porada, S. On-Line Method to Study Dynamics of Ion Adsorption from Mixtures of Salts in Capacitive Deionization. *Desalination* **2016**, *390*, 47−52.
(30) Biesheuvel, P. M.; Fu, Y.; Bazant, M. Z. Electrochemistry and Capacitive Charging of Porous Electrodes in Asymmetric Multicomponent Electrolytes. *Russ. J. Electrochem.* **2012**, *48* (6), 580−592.
(31) Suss, M. E. Size-Based Ion Selectivity of Micropore Electric Double Layers in Capacitive Deionization Electrodes. *J. Electrochem. Soc.* **2017**, *164* (9), E270−E275.
(32) Tang, W.; Kovalsky, P.; He, D.; Waite, T. D. Fluoride and Nitrate Removal from Brackish Groundwaters by Batch-Mode Capacitive Deionization. *Water Res.* **2015**, *84*, 342−349.
(33) Hassanvand, A.; Chen, G. Q.; Webley, P. A.; Kentish, S. E. A Comparison of Multicomponent Electrosorption in Capacitive Deionization and Membrane Capacitive Deionization. *Water Res.* **2018**, *131*, 100−109.
(34) Huang, Z.; Lu, L.; Cai, Z.; Ren, Z. J. Individual and Competitive Removal of Heavy Metals Using Capacitive Deionization. *J. Hazard. Mater.* **2016**, *302*, 323−331.
(35) Hou, C.; Taboada-Serrano, P.; Yiacoumi, S.; Tsouris, C. Electrosorption Selectivity of Ions from Mixtures of Electrolytes inside Nanopores. *J. Chem. Phys.* **2008**, *129*, 224703.
(36) Biesheuvel, P. M.; van Soestbergen, M. Counterion Volume Effects in Mixed Electrical Double Layers. *J. Colloid Interface Sci.* **2007**, *316* (2), 490−499.
(37) Cohen, I.; Avraham, E.; Noked, M.; Soffer, A.; Aurbach, D. Enhanced Charge Efficiency in Capacitive Deionization Achieved by Surface-Treated Electrodes and by Means of a Third Electrode. *J. Phys. Chem. C* **2011**, *115* (40), 19856−19863.
(38) Yang, J.; Zou, L.; Choudhury, N. R. Ion-Selective Carbon Nanotube Electrodes in Capacitive Deionisation. *Electrochim. Acta* **2013**, *91*, 11−19.
(39) Andelman, M. Ionic Group Derivitized Nano Porous Carbon Electrodes for Capacitive Deionization. *J. Mater. Chem. Eng.* **2014**, *2*, 16−22.
(40) Wu, T.; Wang, G.; Dong, Q.; Qian, B.; Meng, Y.; Qiu, J. Asymmetric Capacitive Deionization Utilizing Nitric Acid Treated Activated Carbon Fiber as the Cathode. *Electrochim. Acta* **2015**, *176*, 426−433.
(41) Gao, X.; Omosebi, A.; Landon, J.; Liu, K. Surface Charge Enhanced Carbon Electrodes for Stable and Efficient Capacitive Deionization Using Inverted Adsorption-Desorption Behavior. *Energy Environ. Sci.* **2015**, *8* (3), 897−909.
(42) Biesheuvel, P. M.; Hamelers, H. V. M.; Suss, M. E. Theory of Water Desalination by Porous Electrodes with Immobile Chemical Charge. *Colloids Interface Sci. Commun.* **2015**, *9* (2015), 1−5.
(43) Gao, X.; Porada, S.; Omosebi, A.; Liu, K. L.; Biesheuvel, P. M.; Landon, J. Complementary Surface Charge for Enhanced Capacitive Deionization. *Water Res.* **2016**, *92*, 275−282.
(44) Hemmatifar, A.; Oyarzun, D. I.; Palko, J. W.; Hawks, S. A.; Stadermann, M.; Santiago, J. G. Equilibria Model for PH Variations and Ion Adsorption in Capacitive Deionization Electrodes. *Water Res.* **2017**, *122*, 387−397.
(45) Boublík, T. Hard-Sphere Equation of State. *J. Chem. Phys.* **1970**, *53*, 471.
(46) Mansoori, G. A.; Carnahan, N. F.; Starling, K. E.; Leland, T. W., Jr. Equilibrium Thermodynamic Properties of the Mixture of Hard Spheres. *J. Chem. Phys.* **1971**, *54* (4), 1523−1525.
(47) Bazant, M. Z.; Kilic, M. S.; Storey, B. D.; Ajdari, A. Towards an Understanding of Induced-Charge Electrokinetics at Large Applied Voltages in Concentrated Solutions. *Adv. Colloid Interface Sci.* **2009**, *152*, 48−88.
(48) Giera, B.; Henson, N.; Kober, E. M.; Shell, M. S.; Squires, T. M. Electric Double-Layer Structure in Primitive Model Electrolytes: Comparing Molecular Dynamics with Local-Density Approximations. *Langmuir* **2015**, *31* (11), 3553−3562.
(49) Biesheuvel, P. M. Activated Carbon Is an Electron-Conducting Amphoteric Ion Adsorbent. *arXiv* **2015**, 1509.06354.
(50) Dykstra, J. E.; Keesman, K. J.; Biesheuvel, P. M.; van der Wal, A. Theory of PH Changes in Water Desalination by Capacitive Deionization. *Water Res.* **2017**, *119*, 178−186.
(51) Biesheuvel, P. M.; Porada, S.; Levi, M.; Bazant, M. Z. Attractive Forces in Microporous Carbon Electrodes for Capacitive Deionization. *J. Solid State Electrochem.* **2014**, *18* (5), 1365−1376.
(52) Porada, S.; Zhao, R.; Van Der Wal, A.; Presser, V.; Biesheuvel, P. M. Review on the Science and Technology of Water Desalination by Capacitive Deionization. *Prog. Mater. Sci.* **2013**, *58* (8), 1388−1442.
(53) Mubita, T. M.; Porada, S.; Biesheuvel, P. M.; van der Wal, A.; Dykstra, J. E. Capacitive Deionization with Wire-Shaped Electrodes. *Electrochim. Acta* **2018**, *270*, 165−173.
(54) Nightingale, E. R. Phenomenological Theory of Ion Solvation. Effective Radii of Hydrated Ions. *J. Phys. Chem.* **1959**, *63* (9), 1381−1387.
(55) Cohen, I.; Avraham, E.; Bouhadana, Y.; Soffer, A.; Aurbach, D. The Effect of the Flow-Regime, Reversal of Polarization, and Oxygen on the Long Term Stability in Capacitive De-Ionization Processes. *Electrochim. Acta* **2015**, *153*, 106−114.
(56) Holubowitch, N.; Omosebi, A.; Gao, X.; Landon, J.; Liu, K. Quasi-Steady-State Polarization Reveals the Interplay of Capacitive and Faradaic Processes in Capacitive Deionization. *ChemElectroChem* **2017**, *4* (9), 2404−2413.
(57) Bouhadana, Y.; Ben-Tzion, M.; Soffer, A.; Aurbach, D. A Control System for Operating and Investigating Reactors: The Demonstration of Parasitic Reactions in the Water Desalination by Capacitive de-Ionization. *Desalination* **2011**, *268* (1−3), 253−261.
(58) Vaný sek, P. Equivalent Conductivity of Electrolytes in Aqueous Solution. In *CRC Handbook of Chemistry and Physics*, 99th ed.; Rumble, J. R., Ed.; CRC Press/Taylor & Francis: Boca Raton, FL, USA, 2018.

DOI: 10.1021/acs.est.8b06954
Environ. Sci. Technol. 2019, 53, 8447−8454